Original paper

Petrology and zircon U–Pb dating combined with Hf isotope study of granitic rocks from the Kuluketage Block (Tarim Craton, NW China)

Qian YUAN [1, 2], Xiao-feng CAO[1, 2], Xin-biao LÜ[1, 2]*, En-lin YANG[1], Xiang-dong WANG[1], Yue-gao LIU[1], Ban-xiao RUAN[1], Munir MOHAMMED-ABDALLA-ADAM[1]

[1] *Faculty of Earth Resources, China University of Geosciences, Wuhan 430074, China*
[2] *State Key Laboratory of Geological Processes and Mineral Resources, China University of Geosciences, Wuhan 430074, China; Lvxb_01@163.com*
* *Corresponding author*

We report the petrology, whole-rock geochemistry, zircon LA-ICP-MS U–Pb chronology and zircon Hf isotopic data of Daxigou granitoids (western part of the Kuluketage Block, NW China) to evaluate their likely petrogenesis and tectonic setting. Zircons from syenogranite can be divided into two groups: 1) those that display oscillatory zoning and high Th/U ratios (average = 1.38), implying their magmatic origin and 2) those that exhibit weak zoning and extremely high U and Pb contents but low Th/U ratios (average = 0.35), resembling zircons that experienced hydrothermal alteration. The zircon LA-ICP-MS U–Pb dating of the two groups of zircons yielded weighted mean ages of 1830 ± 12 Ma (MSWD = 0.78) and 1798 ± 21 Ma (MSWD = 1.6) respectively.

The Daxigou granitoids belong mostly to normal-K and sodium-rich metaluminous calc-alkaline type, systematically enriched in LREE and large ion lithophile elements (LILE, e.g., K, Ba and Rb), but significantly depleted in high field strength elements (HFSE, e.g., Ti, P, Nb, Ta and U). Their εHf(t) values and two-stage Hf model ages range from –7.16 to –5.03 and 2.69 to 2.76 Ga, respectively. Taken together, it is suggested that Daxigou granitoids are of I-type affinity and that they were derived by partial melting of a Neoarchaean TTG (e.g., Tuoge Complex) rocks in a continental-arc environment. These new data, combined with previous regional geological studies, demonstrate that a series of Palaeoproterozoic (*c.* 2.0–1.8 Ga) tectono-magmatic events occurred in Kuluketage Block during the assembly of Columbia.

Keywords: Kuluketage Block, syenogranite, LA-ICP-MS zircon dating, Hf isotopes, Paleoproterozoic
Received: 7 June 2013; accepted: 16 June 2014; handling editor: M. Kohút

1. Introduction

The formation and reworking of early Precambrian continental crust are of great importance in understanding the early evolution of the Earth (Condie 1989, 1994; Rudnick 1995; Hawkesworth and Kemp 2006; Long et al. 2010). The Tarim, as well as the North and South China cratons, constitute three major continental blocks in China and represent an important part of the early crustal evolutionary history of northwest China and adjacent areas (Hu AQ et al. 1997; Lu et al. 2008; Demoux et al. 2009; Xiao and Kusky 2009; Lei et al. 2012). The Tarim Craton has a poorly dated Archaean–Paleoproterozoic basement which sporadically crops out along the margins of the Mesozoic–Cenozoic Tarim Basin (Lu et al. 2002). By contrast, the Kuluketage Block (also spelled as Kuruqtagh or Quruqtagh) on the northeastern margin of the Tarim Craton (Fig. 1a–b) is predominantly composed of the Precambrian basement (Lu et al. 2002, 2008; Wang et al. 2013) and provides a good opportunity to study the Precambrian evolutionary history of the Tarim Craton.

Several tectono-thermal events from Neoarchaean to the latest Neoproterozoic have been determined in this area. However, most of the previous studies have mainly focused on Neoproterozoic magmatism and tectonic evolution related to the break-up of Rodinia (Xu et al. 2005; Luo et al. 2007; Sun and Huang 2007; Lu et al. 2008; Zhu et al. 2008; Zhang et al. 2009; Shu et al. 2010; Cao et al. 2011), e.g., *c.* 800–820 Ma Qiganbulake mafic–ultramafic–carbonatite complex, 820 ± 10 Ma Xingdi granodiorite, 795 ± 10 Ma Taiyangdao granite (Zhang et al. 2007a), *c.* 755 Ma bimodal volcanic rocks in the Xinger area (Xu et al. 2005) and 630–650 Ma mafic dykes in Korla (Zhu et al. 2008).

By contrast, little is known about pre-Neoproterozoic magmatism (especially for Mesoproterozoic–Paleoproterozoic magmatism) and the tectonic evolution of the Kuluketage Block. A few studies that have reported on the Paleoproterozoic magmatism and tectonic evolution in the area, mainly dealt with Nd model ages (Feng et al. 1995) and ages from zircons, detrital (Guo et al. 2003; Hu and Wei 2006; Long et al. 2010; Shu et al.

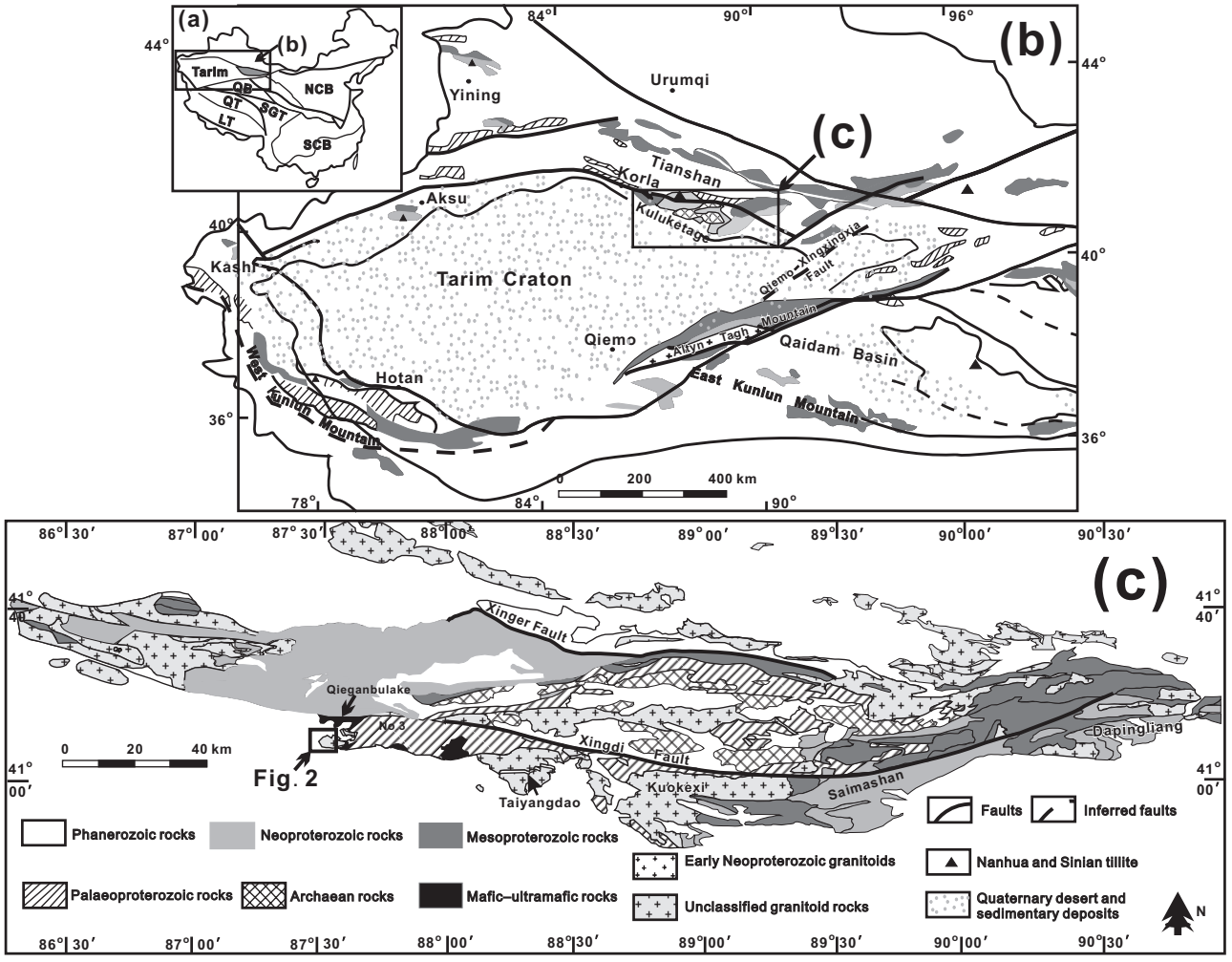

Fig. 1a – Main tectonic domains of China (simplified from Cao et al. 2011). NCB: North China Block, SCB: South China Block, SGT: Songpan–Ganzi Terrane, QB: Qaidam Basin, QT: Qiangtang Terrane, LT: Lhasa Terrane; **b** – Schematic geological map of Tarim Craton and adjacent areas (adopted from Cao et al. 2011); **c** – Schematic geological map of the Kuluketage Block on the northeast margin of the Tarim Craton (Wang et al. 2007).

2010) or metamorphic (Lei et al. 2012). However, no Paleoproterozoic ages of magmatic zircons have been reported yet. Moreover, detailed field observations, precise isotopic ages and high-quality geochemical data are very sparse for late Paleoproterozoic rocks, and this hinders a good understanding of the tectonic evolution of the Tarim Craton, especially the tectonic setting of the Paleoproterozoic magmatism and its relationship to the Palaeo–Mesoproterozoic Columbia Supercontinent (Lei et al. 2012).

Based on detailed field and petrological studies, we report comprehensive geochronological, geochemical and zircon Hf isotope analyses of the Daxigou Complex (syenogranite and granodiorite) in the Kuluketage Block with the aim of characterising its petrogenesis and tectonic setting. Together with regional geology and geochronological data, the Palaeo–Mesoproterozoic assembly of Columbia is being investigated.

2. Geological setting

The Kuluketage Block is composed of two units: the basement which includes Archaean, Paleoproterozoic, Mesoproterozoic and early Neoproterozoic lithologies and the middle Neoproterozoic to Phanerozoic sedimentary cover (Gao et al. 1993; Cheng 1994; Feng et al. 1995; Lu et al. 2008) (Fig. 1b). The Xinger and Xingdi faults are the main regional E–W-oriented structures (Fig. 1c).

Archaean rocks sporadically crop out in the Kuluketage area, known as the Tuoge Complex. It is mainly composed of granitic gneisses with minor amphibolite xenoliths (derived from gabbroic protoliths) (Hu AQ et al. 1999, 2000); it yielded a SHRIMP U–Pb zircon age of 2601 ± 21 Ma (Zhang et al. 2012a) and LA–ICP–MS U–Pb upper intercept zircon age of 2659 ± 15 Ma (Long et al. 2011a). Mostly metasedimentary

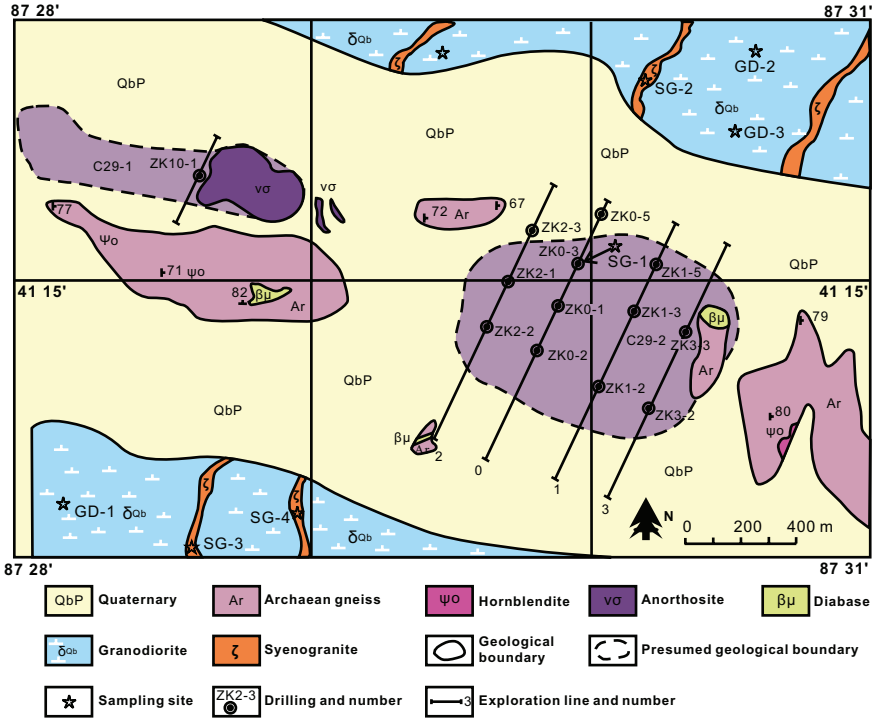

Fig. 2 Geological map of the Daxigou iron–phosphorite deposit in the western Kuluketage (Xia et al. 2010) showing the locations of geochronological and geochemical samples (SG-1 to SG-4: syenogranite; GD-1 to GD-3: granodiorite).

Paleoproterozoic rocks (Xingditage Complex) occur in the western part of the Kuluketage Block. Despite the limited precise geochronology, at the end of the Paleoproterozoic, an important metamorphic event was postulated to have affected Archaean TTG suites and the overlying Paleoproterozoic sedimentary rocks (e.g., Feng et al. 1995; Lu et al. 2002; Zhang et al. 2007b). Mesoproterozoic to early Neoproterozoic low-grade metamorphic rocks, including metamorphosed carbonate and clastic metasedimentary rocks, as well as granitoids, are widespread in the area (Feng et al. 1995; Lu et al. 2008). Middle Neoproterozoic to Phanerozoic rocks consist of mafic dyke swarms, bimodal volcanics as well as fine sandstones, siltstones, shales, dark limestones and chert nodule-bearing dolomites. The mafic dykes with bimodal volcanics were formed at 820–744 Ma and 650–630 Ma (Zhang et al. 2007a; Zhu et al. 2008; Xu et al. 2009). Late Neoproterozoic glacial deposits are also well exposed (Xu et al. 2009).

The Daxigou Complex is the first low-grade, large iron–phosphate deposit discovered at the northern margin of the Tarim Craton (Xia et al. 2010). Several similar complexes with Fe–P mineralization are located along the Xingdi Fault (Xia et al. 2010) and form a strong linear aeromagnetic anomaly (Yuan et al. 2013). From west to east, the petrology of these igneous bodies is as follows: Duosike pyroxenite Complex, Kawuliuketage pyroxenite–hornblendite–syenite Complex, Ao'ertang gabbro–pyroxenite Complex, Daxigou granodiorite–syenogranite Complex and Qieganbulake biotite pyroxenite–carbonate Complex (Xia et al. 2010).

3. Field geology and petrography

The Daxigou Complex is located south of the Xingdi Fault in Kuluketage Block (Fig. 1c) and is controlled by its subsidiary fault. The coordinates of the working area are 87°27'00"–87°31'00"E and 41°12'30"–41°15'30"N. Rocks of this complex are distributed NW–SE over an area of 2.1 × 0.9 km (Fig. 2). They intruded into the Archaean Tuoge Complex which is mainly composed of amphibole-bearing tonalitic gneiss (Xia et al. 2010).

The Daxigou Complex is built mainly by greyish white granodiorite (GD) that exhibits coarse-grained granitic texture and blocky structure. The main mineral components are plagioclase (45–50 vol. %), quartz (25–30 vol. %), K-feldspar (14–17 vol. %), hornblende (8 vol. %), magnetite (1–2 vol. %) and apatite (1 vol. %). Accessory minerals include zircon and ilmenite.

Syenogranites (SG) occur mainly as dykes accompanying the granodiorite, and account for 30 % of the complex. Typically they are pinkish and show massive, medium- to coarse-grained granitic textures. Modal compositions include plagioclase ($An_{35–50}$ 30–50 vol. %), quartz (25–35 vol. %), K-feldspar (18–22 vol. %), biotite (2–5 vol. %), hornblende (1–2 vol. %), and accessory minerals such as apatite, zircon and ilmenite.

Rocks of the Tuoge Complex are composed of plagioclase (40–48 vol. %), quartz (25–30 vol. %), alkali feldspar (25–30 vol. %) and biotite (5–10 vol. %) with some accessory minerals, e.g., titanite, apatite and zircon. Generally, the Tuoge Complex exhibits considerable

weathering in the Daxigou area, rendering it not suitable for chemical analyses.

4. Analytical methods

4.1. Zircon U–Pb dating

Zircon grains were separated using conventional crushing, grinding and wet shaking table methods, followed by heavy liquid (tetrabromomethane) and magnetic separation. Hand-picked zircon grains were mounted in epoxy blocks and polished prior to LA-ICP-MS analysis, the surfaces of grain mounts were washed in dilute HNO_3 and pure alcohol to remove any potential lead contamination. The selection of zircon grains for isotopic analyses was based upon cathodoluminescence (CL) images (Fig. 3). Zircon U–Th–Pb measurements were done at the State Key Laboratory of Geological Processes and Mineral Resources, China University of Geosciences, Wuhan (GPMR-CUGW), using a GeoLas 2005 System. An Agilent 7700a ICP-MS instrument was employed, with a 193 nm ArF-excimer laser (32 μm beam diameter). Details on instrumentation and analytical accuracy were given by Liu et al. (2008, 2010). Time-dependent drifts of U–Th–Pb isotopic ratios were corrected using a linear interpolation (with time) for every five analyses according to the variations of external zircon standard 91500 (i.e., 2× 91500 – 5 samples – 2× 91500) (Liu et al. 2010). The ages were calculated by in-house software ICPMSDataCal (ver 9.0) (Liu et al. 2008), and Concordia diagrams were plotted by Isoplot/Ex ver. 3.0 (Ludwig 2003).

4.2. Whole-rock geochemistry

Rock samples for the major- and trace-element analyses were carefully selected to be representative of geographical distribution of the two different rock types (Fig. 2): four syenogranites and three granodiorites. Whole-rock samples were crushed to 0.5 cm chips in a steel-faced jaw crusher and powdered with an agate mill.

Major elements were analysed with a PAN analytical Axios X-ray fluorescence spectrometer (XRF) at ALS Chemex (Guangzhou) Ltd. A calcined or ignited sample (0.9 g) was added to 9.0 g of lithium borate flux (1 : 1 $Li_2B_4O_7$–$LiBO_2$), mixed well and fused in an auto fluxer between 1050–1100 °C. A flat molten glass disc was prepared and analysed by XRF with a precision better than 5 %.

Trace-element concentrations were determined with an Elan 9000 ICP-MS at the same lab. To the sample powder (0.2 g) was added lithium metaborate flux (0.9 g), mixed well and fused in a furnace at 1000 °C. The resulting melt was then cooled and dissolved in 100 ml of 4 % HNO_3/2 % HCl solution and analyzed by ICP-MS with a precision better than 10 % for all elements.

4.3. In situ zircon Hf isotope analysis

In situ zircon Hf isotopic analyses were conducted using a Neptune Plus MC-ICP-MS, in combination with a Geolas 2005 excimer ArF laser-ablation system, at the GPMR-CUGW. During the analysis, a laser repetition rate of 20 Hz at 200 mJ was used with the spot diameter of 44 μm. Details of the analytical technique were described in (Hu ZC et al. 2012). During the analysis, the $^{176}Hf/^{177}Hf$ ratios of the standard zircon (GJ-1) were 0.282013 ± 0.000022 (2σ, n = 276), agreeing with the recommended values (Woodhead and Hergt 2005; Wu FY et al. 2006; Sláma et al. 2008; Li et al. 2010) within 2σ error. Off-line selection and integration of analytical signals, and isobaric interference and mass fractionation correction of Lu–Hf isotopic ratios were also performed by the ICPMS-DataCal.

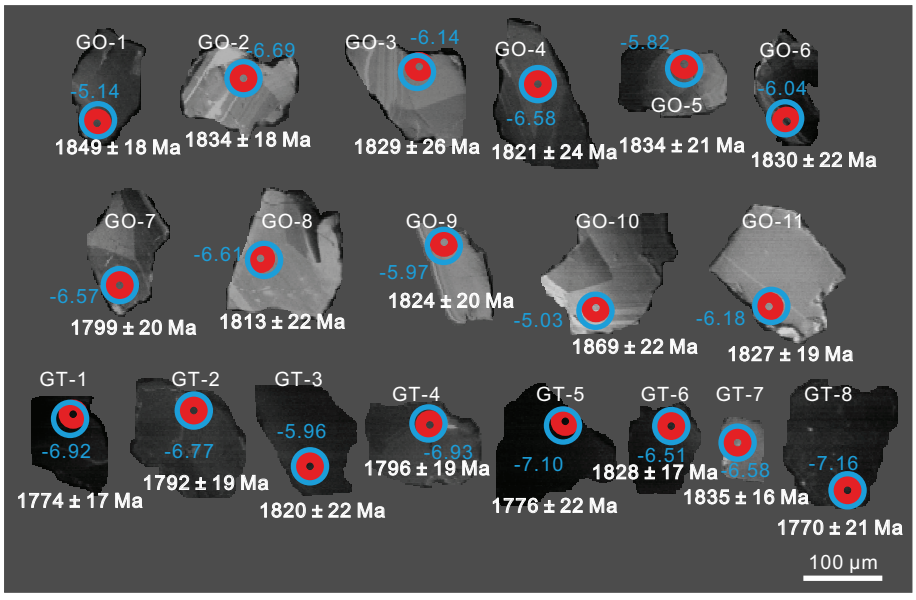

Fig. 3 Cathodoluminescence (CL) images of zircons from the syenogranite SG-2. LA-ICP-MS U–Pb (red circles) and *in situ* Hf determination spots (bigger circles) with $^{207}Pb/^{235}U$ ages and εHf(t) values are indicated.

5. Analytical results

5.1. Zircon U–Pb geochronology

Zircons are relatively abundant in the dated syenogranite sample SG-2 (Fig. 2). According to the shape, colour and length/width ratios, they can be categorised into two groups, distinguished below. The measured Pb isotopic ratios and calculated ages for 19 analyses on 19 zircon crystals are given in Tab. 1.

5.1.1. Group one (igneous) zircons

Group one (GO) zircons are sub-euhedral, short to long prismatic, and transparent, and their length/width ratios are *c.* 2.7. In CL images (Fig. 3; upper two rows), they exhibit oscillatory zoning, a feature typical of magmatic zircon (Corfu et al. 2003), but a few grains show clear core–rim textures (GO-6).

The analyses display variable abundances of U (99–513 ppm), Th (123–622 ppm) and Pb (49–256 ppm) but consistently high Th/U ratios (1.09–2.11) which are suggestive of an igneous origin (Hanchar and Rudnick 1995; Hoskin and Black 2000). This group of closely clustered concordant analyses yields a weighted mean $^{207}Pb/^{235}U$ age of 1830 ± 12 Ma (MSWD = 0.78) (Fig. 4a), which we adopt as the crystallization age of the syenogranite.

5.1.2. Group two (recrystallized) zircons

By contrast, group two (GT) zircons are irregular in shape

Tab. 1 Laser-ablation ICP-MS U–Pb isotopic data for zircon from the dated syenogranite

Sample	Concentrations (ppm)				U–Th–Pb isotopic ratios						Ages (Ma)					
spot	Pb	Th	U	Th/U	$^{207}Pb/^{206}Pb$	1σ	$^{207}Pb/^{235}U$	1σ	$^{206}Pb/^{238}U$	1σ	$^{207}Pb/^{206}Pb$	1σ	$^{207}Pb/^{235}U$	1σ	$^{206}Pb/^{238}U$	1σ
GO-1	152.0	553	262	2.11	0.1088	0.0022	5.1793	0.1067	0.3411	0.0030	1789	36	1849	18	1892	14
GO-2	145.4	363	282	1.29	0.1056	0.0022	5.0890	0.1078	0.3452	0.0031	1726	39	1834	18	1912	15
GO-3	49.7	130	99	1.31	0.1068	0.0034	5.0600	0.1560	0.3404	0.0039	1746	57	1829	26	1889	19
GO-4	256.0	622	513	1.21	0.1036	0.0029	5.0081	0.1391	0.3454	0.0034	1700	52	1821	24	1912	16
GO-5	169.1	457	325	1.41	0.1057	0.0027	5.0851	0.1275	0.3442	0.0035	1728	46	1834	21	1907	17
GO-6	66.9	181	129	1.40	0.1063	0.0027	5.0659	0.1318	0.3407	0.0036	1737	47	1830	22	1890	17
GO-7	151.8	455	286	1.59	0.1071	0.0025	4.8826	0.1138	0.3255	0.0028	1752	44	1799	20	1816	14
GO-8	105.7	246	218	1.13	0.1107	0.0029	4.9628	0.1263	0.3207	0.0031	1811	48	1813	22	1793	15
GO-9	131.8	340	260	1.31	0.1092	0.0026	5.0250	0.1183	0.3287	0.0029	1787	43	1824	20	1832	14
GO-10	55.6	123	113	1.09	0.1129	0.0030	5.3033	0.1385	0.3373	0.0036	1847	48	1869	22	1873	17
GO-11	128.5	333	257	1.30	0.1113	0.0025	5.0454	0.1138	0.3257	0.0030	1820	36	1827	19	1818	15
Average	128.4	345.7	249.5	1.38	□	□	□	□	□	□	□	□	□	□	□	□
GT-1	820.0	293	2248	0.13	0.1041	0.0021	4.7391	0.0965	0.3257	0.0029	1698	69	1774	17	1817	14
GT-2	488.0	598	1216	0.49	0.1056	0.0023	4.8428	0.1084	0.3280	0.0031	1726	41	1792	19	1828	15
GT-3	356.3	392	841	0.47	0.1038	0.0028	5.0067	0.1323	0.3444	0.0034	1692	49	1820	22	1908	16
GT-4	952.0	546	2411	0.23	0.1056	0.0024	4.8638	0.1094	0.3288	0.0030	1724	41	1796	19	1833	14
GT-5	1146.1	493	3024	0.16	0.1052	0.0027	4.7483	0.1224	0.3217	0.0034	1718	47	1776	22	1798	17
GT-6	242.2	302	569	0.53	0.1091	0.0024	5.0494	0.1114	0.3308	0.0030	1785	40	1828	19	1842	15
GT-7	203.8	290	466	0.62	0.1087	0.0027	5.0934	0.1284	0.3349	0.0034	1789	51	1835	21	1862	16
GT-8	936.0	471	2354	0.20	0.1089	0.0028	4.7151	0.1199	0.3100	0.0033	1781	14	1770	21	1741	16
Average	643.1	423.1	1641.1	0.35	□	□	□	□	□	□	□	□	□	□	□	□

GO = group one; GT = group two

and orange in colour under the optical microscope; their length/width ratios are *c.* 1.2. In CL images (Fig. 3, the bottom row), they are much darker than magmatic rims and exhibit no zoning. This suggests that they may have undergone hydrothermal alteration, similar to the zircons in alkali syenites (Corfu et al. 2003).

The group two zircons show much higher U (466–3024 ppm), Pb (204–1146 ppm) and total REE contents, but lower Th/U ratios (0.13–0.62) than those of group one (Tab. 1). However, they show $^{176}Lu/^{177}Hf$ and $^{176}Hf/^{177}Hf(t)$ ratios identical to the GO zircons (see Tab. 3). These characteristics are similar to those of zircons formed by alteration with an aqueous fluid or a hydrous melt (e.g., Gerdes and Zeh 2009). Eight analyses of eight irregular grains with bad oscillatory zoning yielded a weighted mean $^{207}Pb/^{235}U$ age of 1798 ± 21 Ma (MSWD = 1.6, 2σ) (Fig. 4b), i.e. postdating by nearly 30 Ma the intrusion (GO). Thus we interpreted this datum as the age of post-magmatic alteration.

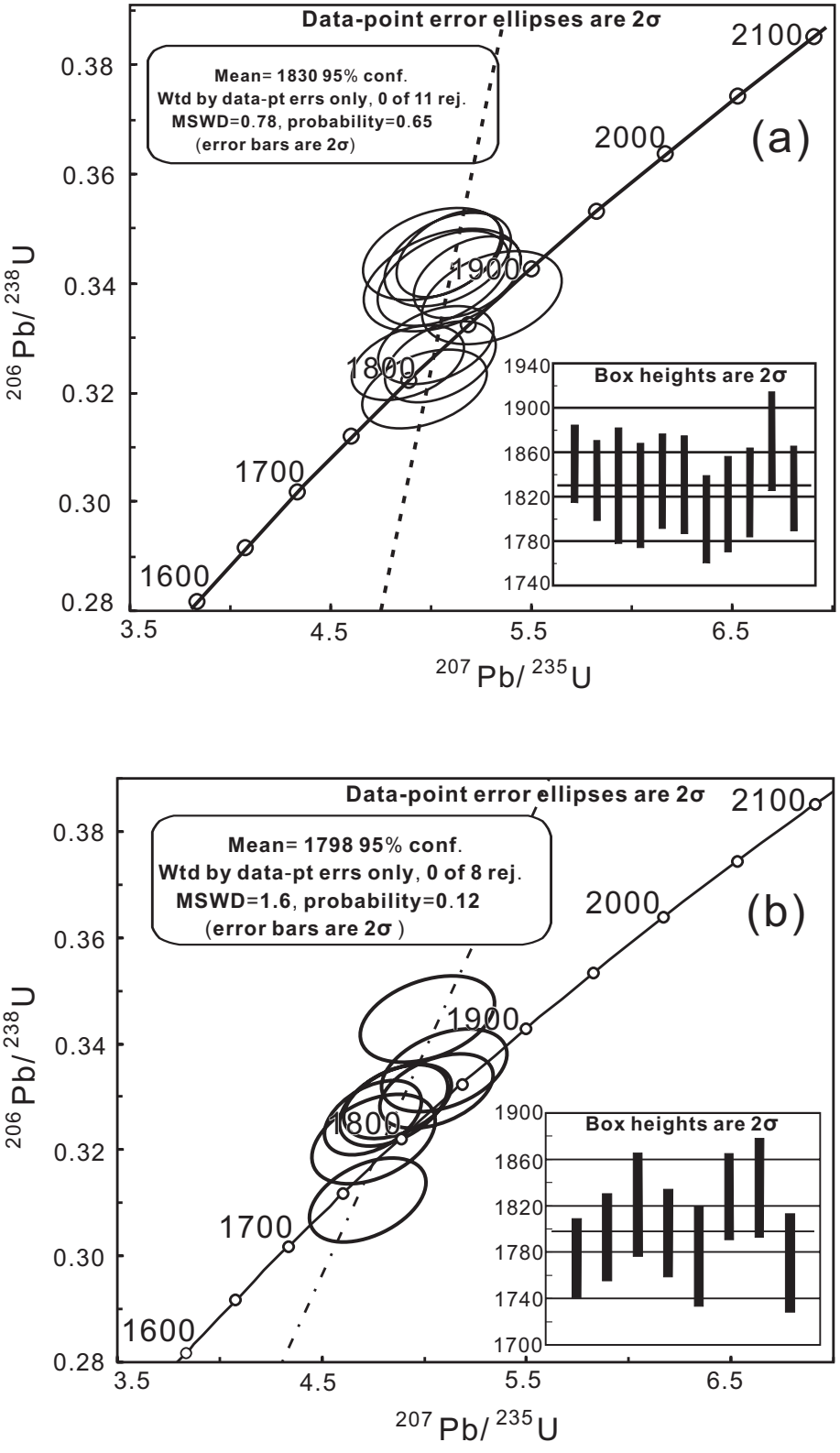

Fig. 4 U–Pb Concordia plots and recalculated weighted mean $^{207}Pb/^{235}U$ ages of group one zircons (**a**) and group two zircons (**b**) are given in the text box.

5.2. Major elements

The representative whole-rock major- and trace-element compositions are given in Tab. 2, including those for the Tuoge Complex. In addition, these samples may have undergone some degree of alteration, such as chloritization, even though their LOI values are moderate (2.09–3.63 wt. %), except the sample SG-3 (6.58 wt. %).

The syenogranites are characterised by variable SiO_2 (60.44–73.28 wt. %), K_2O (1.05–6.23 wt. %), high Na_2O (3.17–5.62 wt. %), and low P_2O_5 (0.014–0.113 wt. %), TiO_2 (0.03–0.43 wt. %) with MgO (0.24–1.66 wt. %). After rejection of the K-rich sample (SG-1), the Na_2O/K_2O ratios range from 1.19 to 5.35, i.e. are characteristic of I-type granites

Tab. 2 Major- (wt. %) and trace-element data (ppm, including REE) from the Daxigou granitoids (this work) and Tuoge Complex (Long et al. (2010)

Sample No.	SG-1	SG-2	SG-3	SG-4	GD-1	GD-2	GD-3	TC-1	TC-2	TC-3	TC-4
Lithology	Syenogranite				Granodiorite			Tuoge Complex			
SiO_2	69.83	73.28	60.44	68.86	69.25	72.05	61.85	69.30	68.90	71.00	66.30
Al_2O_3	14.22	12.23	14.46	12.75	12.61	12.43	14.98	13.50	13.60	13.10	14.40
$Fe_2O_{3(T)}$	0.52	3.38	4.38	1.60	5.08	2.70	6.90	4.06	4.50	3.69	4.94
CaO	2.17	0.96	4.58	4.23	1.46	2.07	3.59	2.57	2.50	0.98	2.74
MgO	0.24	1.40	1.66	0.39	1.79	0.91	2.30	0.97	1.36	1.26	1.71
Na_2O	3.17	3.87	5.62	4.05	4.45	5.16	4.21	3.72	3.63	4.54	3.30
K_2O	6.23	2.59	1.05	3.40	1.49	1.43	1.02	3.00	2.68	3.34	3.43
TiO_2	0.03	0.08	0.43	0.03	0.22	0.26	0.94	0.81	0.86	0.56	0.89
MnO	<0.01	0.05	0.07	0.02	0.07	0.04	0.06	0.08	0.08	0.09	0.07
P_2O_5	0.01	0.03	0.11	0.02	0.09	0.09	0.35	0.25	0.25	0.19	0.31
SrO	0.02	0.02	0.04	0.03	0.02	0.03	0.07	–	–	–	–
BaO	0.13	0.07	0.08	0.09	0.10	0.05	0.10	–	–	–	–
LOI	2.46	2.09	6.58	3.63	2.57	2.44	2.80	1.23	1.10	0.83	1.32
∑	99.02	100.05	99.50	99.10	99.19	99.65	99.17	99.50	99.50	99.60	99.40
Na_2O/K_2O	0.51	1.49	5.35	1.19	2.99	3.61	4.13	1.24	1.35	1.36	0.96
Na_2O+K_2O	9.40	6.46	6.67	7.45	5.94	6.59	5.23	6.72	6.31	7.88	6.73
A/NK	1.19	1.33	1.39	1.23	1.41	1.24	1.87	1.44	1.53	1.18	1.58
A/CNK	0.89	1.12	0.77	0.71	1.09	0.90	1.03	0.96	1.01	1.02	1.02
δ	3.29	1.38	2.55	2.15	1.34	1.49	1.45	1.72	1.54	2.22	1.94
Co	82.50	78.20	33.70	64.40	22.60	46.70	41.90	4.38	6.58	6.34	6.67
Ni	10.00	9.00	17.00	8.00	10.00	10.00	26.00	5.67	3.82	6.65	7.39
Rb	126.5	52.9	23.2	67.8	30.5	30.2	13.4	48.6	61.7	39.9	69.5
Ba	1205	699	739	828	957	554	887	2206	2044	1974	2586
Th	0.58	4.14	4.77	3.42	8.4	4.62	0.47	7.81	7.80	11.07	14.96
U	0.25	0.59	0.69	1.01	0.51	0.47	0.44	0.52	0.52	0.44	0.50
K	51715.9	21499.9	8716.2	28223.7	12368.6	11870.6	8467.1	24911.3	22254.1	27734.6	28481.9
La	3.6	9.2	38.8	6.8	28.0	21.8	35.3	108.0	116.0	110.0	153.0
Ce	6.6	15.5	70.7	13.1	53.8	41.7	78.1	236.0	250.0	232.0	304.0
Pb	18.00	10.00	6.00	13.00	5.00	9.00	25.00	17.58	10.97	9.93	13.23
Pr	0.65	1.62	7.33	1.52	5.80	4.36	9.77	28.00	29.70	28.00	32.30
Sr	223	206	370	283	207	241	682	346	265	140	436
P	61.50	140.57	496.40	96.64	421.72	395.36	1550.69	1091.34	1091.34	829.42	1353.26
Nd	2.30	6.00	26.60	5.90	20.70	16.20	41.00	102.00	106.00	98.70	109.00
Ta	0.40	0.30	0.50	0.50	0.30	0.30	0.30	1.14	0.77	0.53	0.65
Zr	41	45	209	46	145	143	281	408	253	300	310
Hf	1.70	1.30	5.40	1.70	4.20	4.60	6.60	10.25	6.23	7.57	7.70
Sm	0.45	1.04	4.26	1.42	3.81	3.27	7.34	17.20	16.40	15.00	13.20
Eu	0.50	0.51	1.16	0.75	1.09	0.81	2.06	3.53	3.37	2.63	2.70
Ti	143.65	383.06	2058.96	143.65	1053.42	1244.95	4500.98	4856.25	5156.01	3357.40	5335.88
Gd	0.36	1.05	3.64	1.60	3.15	4.01	6.09	14.10	13.00	10.50	10.00
Tb	0.05	0.18	0.46	0.26	0.48	0.64	0.72	2.14	1.79	1.49	1.05
Dy	0.25	1.03	2.54	1.56	3.06	3.66	3.56	12.00	9.65	7.92	4.98
Y	1.6	5.9	14.2	10.6	16.8	19.5	16.2	59.5	46.9	38.1	22.7
Nb	1.0	1.4	9.8	4.3	4.1	5.9	5.4	18.5	18.1	11.6	10.1
Ho	0.05	0.21	0.47	0.33	0.60	0.69	0.60	2.38	1.81	1.47	0.89
Er	0.14	0.64	1.34	1.07	1.65	2.03	1.62	6.42	4.63	3.68	2.21
Tm	0.03	0.09	0.20	0.16	0.28	0.29	0.20	0.92	0.62	0.47	0.30
Yb	0.15	0.69	1.32	1.13	1.60	1.93	1.16	5.88	3.80	2.71	1.77
Lu	0.03	0.10	0.20	0.19	0.24	0.28	0.16	0.86	0.53	0.35	0.26
ΣREE	15.16	37.86	159.02	35.79	124.26	101.67	187.68	539.43	557.30	514.92	635.66
LREE	14.10	33.87	148.85	29.49	113.20	88.14	173.57	494.73	521.47	486.33	614.20
HREE	1.06	3.99	10.17	6.30	11.06	13.53	14.11	44.70	35.83	28.59	21.46
LREE/HREE	13.30	8.49	14.64	4.68	10.24	6.51	12.30	11.07	14.55	17.01	28.62
La_N/Yb_N	17.22	9.56	21.08	4.32	12.55	8.10	21.83	13.17	21.90	29.12	62.00
δEu	3.80	1.49	0.90	1.52	0.96	0.68	0.94	0.69	0.71	0.64	0.72

Note: data of Tuoge Complex are from Long et al (2010).

A/NK = molar ratio of $Al_2O_3/(Na_2O + K_2O)$; A/CNK = molar ratio of $Al_2O_3/(CaO + Na_2O + K_2O)$ (Shand 1943);

$\delta = [w(K_2O + Na_2O)^2]/[w(SiO_2 - 43)]$ (Rittmann 1953); $\delta Eu = Eu/Eu^* = Eu_N/\sqrt{Sm_N + Gd_N}$

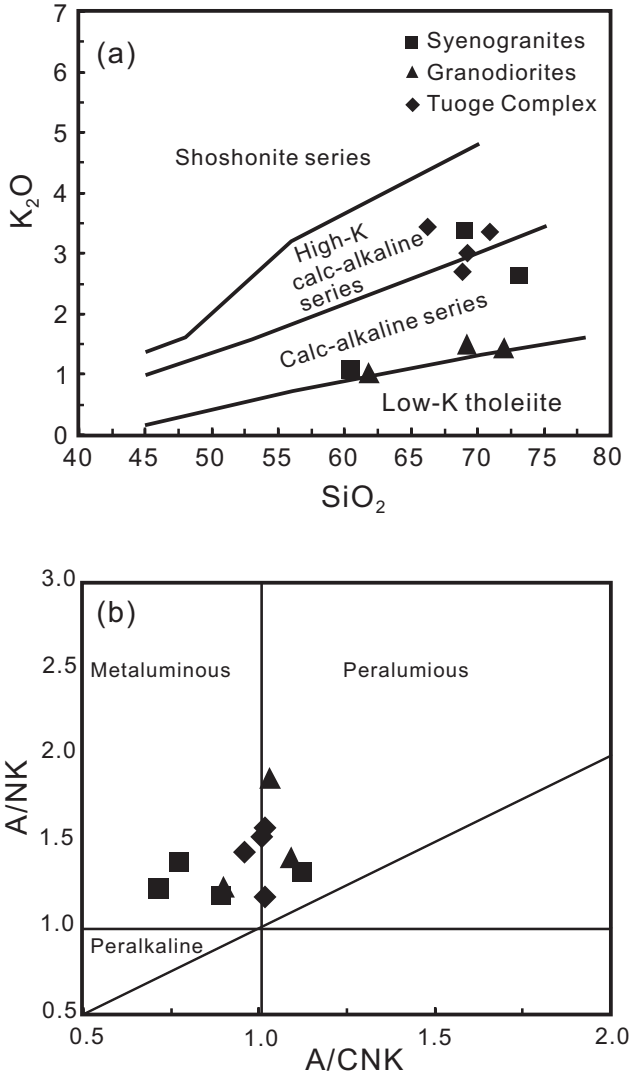

Fig. 5a – Diagram of K_2O–SiO_2 for granitoids of the Daxigou and Tuoge complexes (Peccerillo et al. 1976). **b** – Diagram of A/NK–A/CNK for the same rocks (Shand 1943).

(Chappell and White 1974). Silica alkalic indexes (δ) [wt. % $(K_2O + Na_2O)^2$] / [wt. % (SiO_2 – 43)] (Rittmann 1953) range from 1.37 to 3.29, which suggests calc-alkaline characteristics. In addition, most of the data fall in the medium-K, calc-alkaline field on the SiO_2 versus K_2O diagram of Peccerillo and Taylor (1976) (Fig. 5a). The rocks are metaluminous, with the A/CNK [molar Al_2O_3 /(CaO + K_2O + Na_2O)] varying from 0.71 to 0.93, except sample SG-2 (A/CNK = 1.12) (Fig. 5b, Shand 1943).

The Daxigou granodiorites contain 61.85–72.05 wt. % SiO_2, 12.61–14.98 wt. % Al_2O_3, 1.46 %–3.59 wt. % CaO, 0.91–2.3 wt. % MgO and 1.02–1.49 wt. % K_2O, with Na_2O/K_2O ratios of 2.99–4.13 and low silica alkalic indexes (δ = 1.34–1.49). All granodiorites belong to the calc-alkaline series (Fig. 5a) and are subaluminous (A/CNK = 0.90–1.09) (Fig. 5b).

The Tab. 2 and Harker plots (Fig. 6) show that the average compositions of syenogranite and granodiorite are similar, with small differences in $Fe_2O_{3(t)}$ content. Moreover, compared with the Tuoge Complex, the Daxigou granitoids contain rocks with a slightly higher Na_2O and a lower FeOt contents; SiO_2, Al_2O_3, CaO and MgO contents are comparable. In the Harker diagrams, the three rock types show consistent negative correlations between SiO_2 and Al_2O_3, Fe_2O_3t, CaO, MgO and P_2O_5. Laboratory studies have shown the different behaviour of apatite in I-type (Wolf and London 1994) and S-type granites, and this has been successfully used to distinguish granite types (Chappell 1999). Most of our data show that Daxigou granitoids are metaluminous, and the content of P_2O_5 is low and negatively correlated with SiO_2 (Fig. 6), which corresponds to the evolutionary trend of I-type granites (Chappell and White 1992). Therefore, we suggest that Daxigou granitoids are of I-type affinity and may have a genetic relationship with the Tuoge Complex.

5.3. Trace elements

The trace-element concentrations of the Daxigou granitoids are highly variable. However, most show mutually comparable patterns in primitive mantle-normalized spider diagram (Fig. 7a). Most of the trace-element contents of granodiorites are higher than those of syenogranites but lower than those of the Tuoge Complex. Generally, all the samples are enriched in large ion lithophile elements (LILE, e.g., K, Ba and Rb) but depleted in high field strength elements (HFSE, e.g., Ti, P, Nb, Ta and U) (Fig. 7a), and thus show distribution patterns resembling volcanic-arc rocks. We suggest that Ba was elevated by either K-feldspar or biotite accumulation or, along with Rb and K, during hydrothermal alteration.

The chondrite-normalised REE patterns (Fig. 7b) for the granodiorites and the Tuoge Complex have weak to moderate negative Eu anomalies (Eu/Eu* = 0.64–0.96, calculation method in Tab. 2), whereas the syenogranites show weak negative to moderately positive Eu anomalies (Eu/Eu* = 0.90–3.80). Nevertheless, most samples share similar chondrite-normalised REE patterns enriched in LREE over HREE (Fig. 7b).

5.4. In situ zircon Hf isotopic compositions

The zircons of both groups were analysed for their Lu–Hf isotopic compositions on the dated domains (Fig. 3), and the data are presented in Tab. 3 and graphically illustrated in Fig. 8. Table 3 shows that the $^{176}Lu/^{177}Hf$ ratios of all zircons are less than 0.002, which indicates that they accumulated little radiogenic Hf since they formed.

Eleven analyses obtained from the GO zircons yielded rather variable εHf(t) values of –6.69 to –5.03 (Tab. 3),

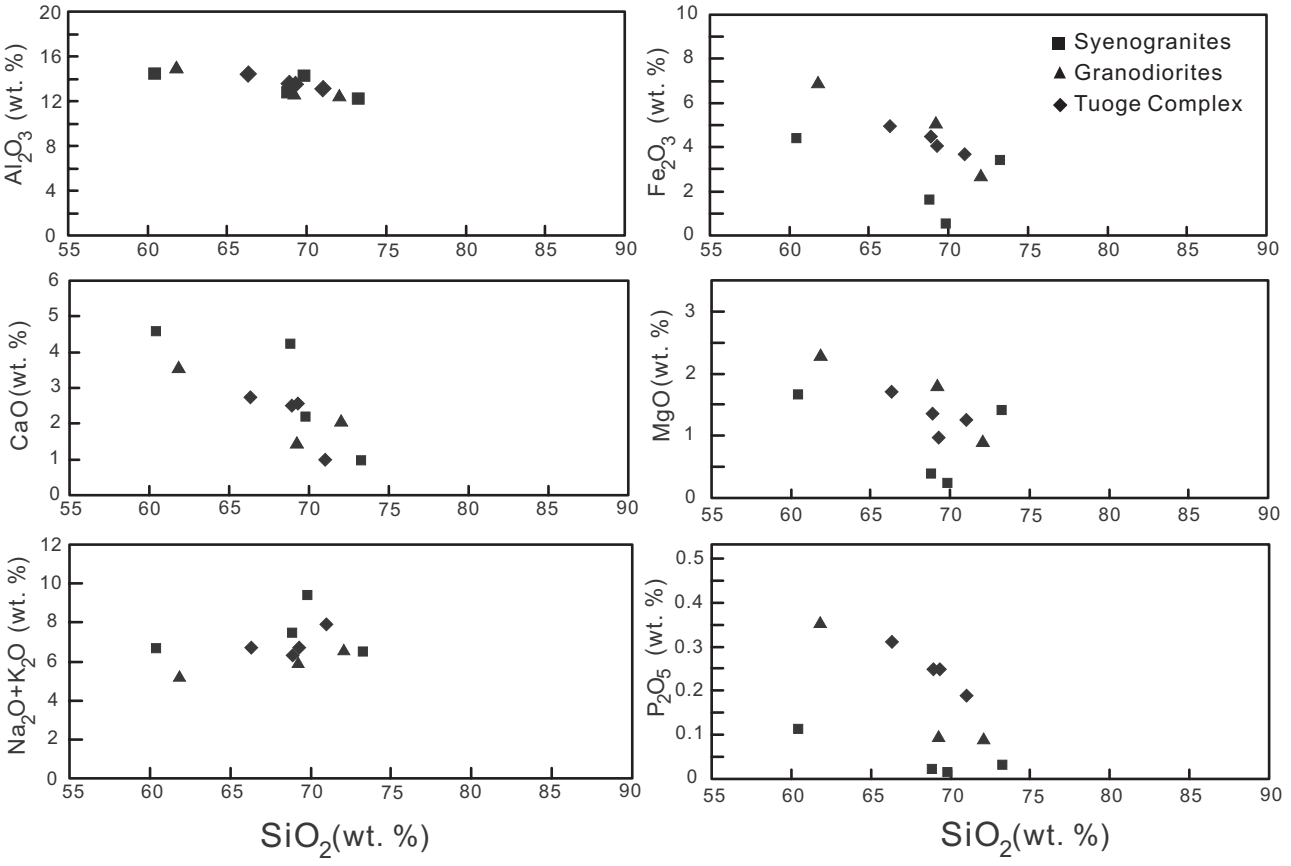

Fig. 6 Harker diagrams for granitoids of the Daxigou and Tuoge complexes.

Tab. 3 Zircon Lu–Hf isotopic compositions for the syenogranite from Daxigou granitoids

Spot	Age (Ma)	$^{176}Hf/^{177}Hf$	1σ	$^{176}Lu/^{177}Hf$	1σ	$^{176}Yb/^{177}Hf$	1σ	εHf(0)	$f_{Lu/Hf}$	εHf(t)	T_{DM1}	T_{DM2}
GO-01	1849	0.281492	0.000014	0.000886	0.000011	0.030306	0.000169	–45.25	–0.97	–5.14	2.45	2.69
GO-02	1834	0.281442	0.000011	0.000418	0.000002	0.013939	0.000137	–47.04	–0.99	–6.69	2.49	2.76
GO-03	1829	0.281481	0.000012	0.001018	0.000001	0.032573	0.000105	–45.65	–0.97	–6.14	2.48	2.73
GO-04	1821	0.281455	0.000013	0.000475	0.000002	0.015776	0.000033	–46.58	–0.99	–6.58	2.48	2.75
GO-05	1834	0.281488	0.000012	0.001045	0.000001	0.034317	0.000117	–45.40	–0.97	–5.82	2.47	2.72
GO-06	1830	0.281471	0.000013	0.000655	0.000001	0.022488	0.000080	–46.02	–0.98	–6.04	2.47	2.73
GO-07	1799	0.281465	0.000011	0.000366	0.000004	0.012501	0.000192	–46.21	–0.99	–6.57	2.46	2.73
GO-08	1813	0.281475	0.000010	0.000917	0.000004	0.031709	0.000227	–45.88	–0.97	–6.61	2.48	2.74
GO-09	1824	0.281474	0.000011	0.000571	0.000001	0.019712	0.000086	–45.92	–0.98	–5.97	2.46	2.72
GO-10	1869	0.281478	0.000014	0.000751	0.000003	0.027590	0.000050	–45.76	–0.98	–5.03	2.46	2.70
GO-11	1827	0.281466	0.000012	0.000581	0.000001	0.020215	0.000065	–46.19	–0.98	–6.18	2.47	2.73
GT-01	1774	0.281503	0.000013	0.001312	0.000002	0.041417	0.000174	–44.87	–0.96	–6.92	2.47	2.73
GT-02	1792	0.281486	0.000011	0.001004	0.000004	0.033979	0.000182	–45.48	–0.97	–6.77	2.47	2.74
GT-03	1820	0.281487	0.000013	0.000882	0.000001	0.030499	0.000060	–45.44	–0.97	–5.96	2.46	2.71
GT-04	1796	0.281465	0.000012	0.000601	0.000004	0.020357	0.000114	–46.21	–0.98	–6.93	2.47	2.75
GT-05	1776	0.281509	0.000011	0.001669	0.000002	0.055547	0.000179	–44.66	–0.95	–7.10	2.48	2.74
GT-06	1828	0.281456	0.000010	0.000591	0.000001	0.020237	0.000052	–46.52	–0.98	–6.51	2.48	2.75
GT-07	1835	0.281455	0.000010	0.000739	0.000001	0.025285	0.000078	–46.56	–0.98	–6.58	2.49	2.76
GT-08	1770	0.281514	0.000011	0.001752	0.000003	0.059155	0.000161	–44.50	–0.95	–7.16	2.48	2.74

GO = group one; GT = group two. $\varepsilon_{Hf}(t) = \{[(^{176}Hf/^{177}Hf)_s - (^{176}Lu/^{177}Hf)_s \times (e^{\lambda t} - 1)]/[(^{176}Hf/^{177}Hf)_{CHUR,0} - (^{176}Lu/^{177}Hf)_{CHUR} \times (e^{\lambda t} - 1)] - 1\} \times 10000$; s = sample, $(^{176}Hf/^{177}Hf)_{CHUR,0} = 0.282772$, $(^{176}Lu/^{177}Hf)_{CHUR} = 0.0332$, $(^{176}Hf/^{177}Hf)_{DM} = 0.28325$, $(^{176}Lu/^{177}Hf)_{DM} = 0.0384$ (according to Blichert-Toft and Albarède 1997; Griffin et al. 2000), t = the crystallization age of zircon, $\lambda = 1.867 \times 10^{-11}$ a^{-1} (Söderlund et al. 2004), $(^{176}Lu/^{177}Hf)_C = 0.015$, S and DM are the upper continental crust, the sample and the depleted mantle, respectively.

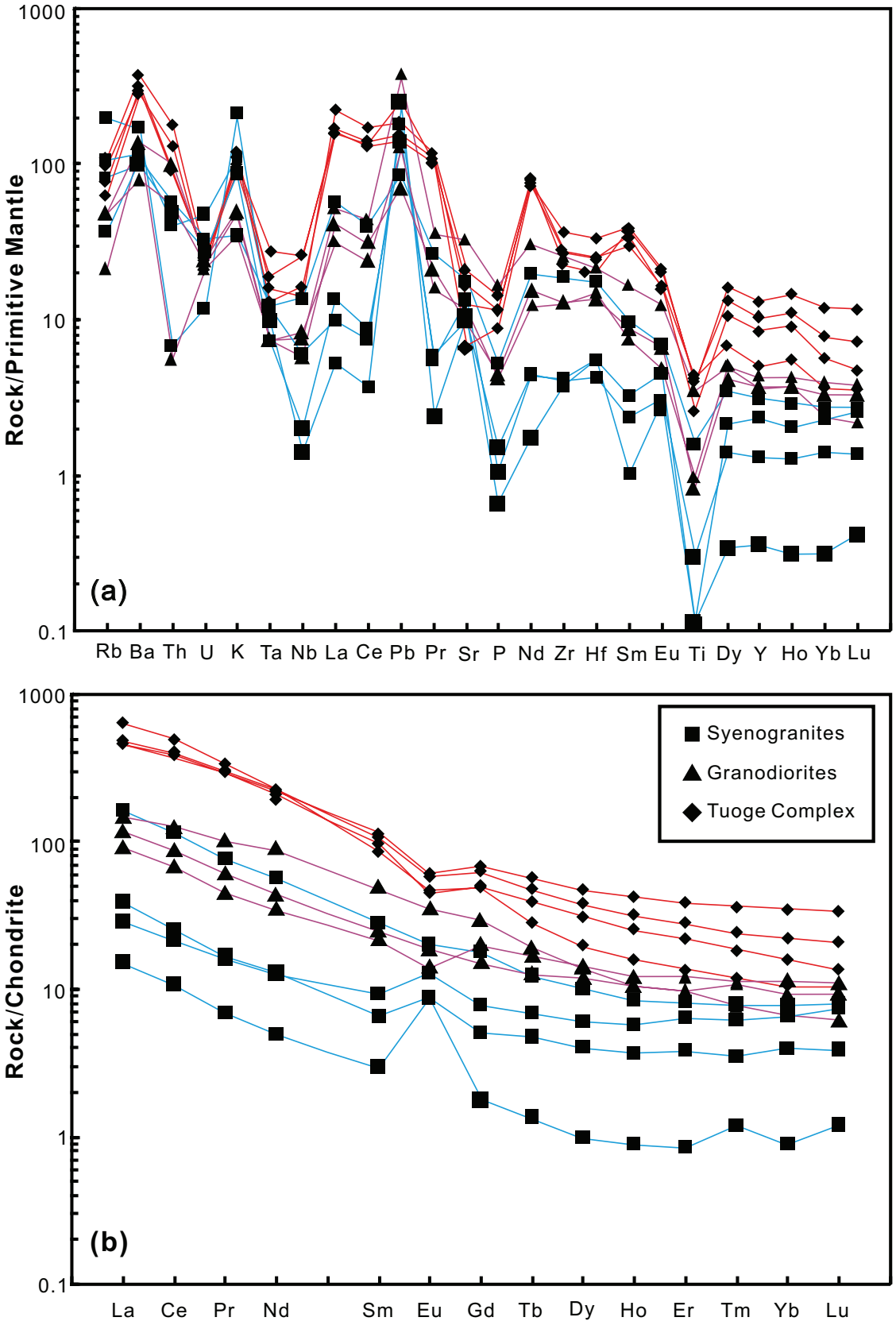

Fig. 7 Primitive mantle-normalized trace-element patterns (**a**) and chondrite-normalized REE patterns (**b**) for the Daxigou granitoids and Tuoge Complex. Normalization data are from Sun and McDonough (1989).

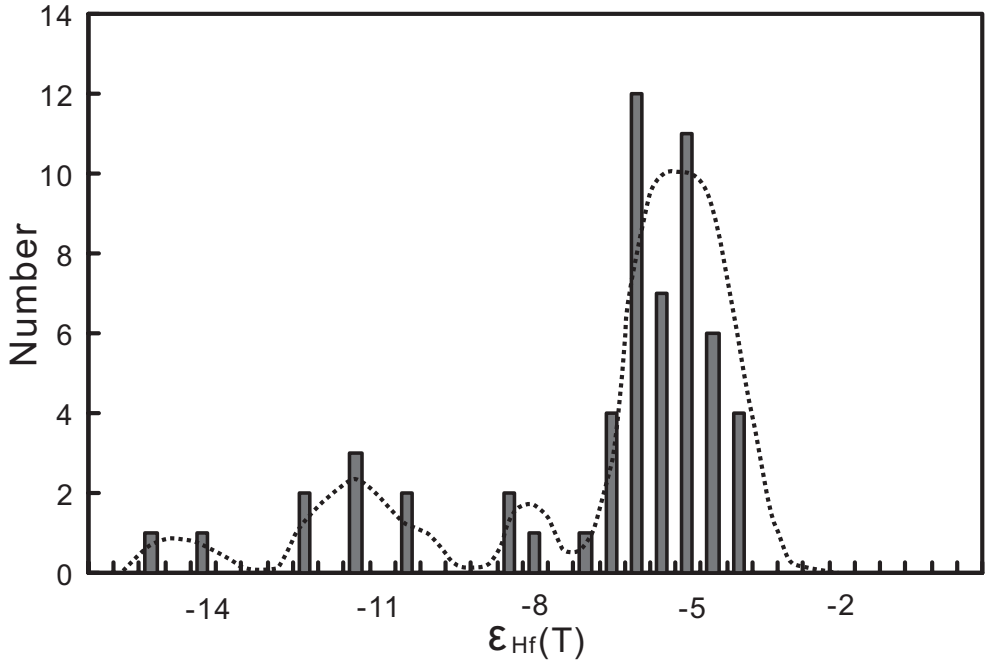

Fig. 8 Frequency histogram of εHf(t) values for zircons of the syenogranite (SG-2).

nearly constant one-stage model ages of 2.45–2.49 Ga and two-stage model ages of 2.69–2.76 Ga. Eight spot analyses for the GT zircons gave εHf(t) values of –7.16 to –5.96, similar one-stage model ages (2.46–2.49 Ga) and two-stage model ages (2.71–2.76 Ga).

Taken together, the studied zircons show a single distribution in εHf(t) values (Fig. 8) with an average of –6.35 (Tab. 3). The Archaean Hf model ages indicate that the studied rocks may have originated from the melting of the Archaean rocks (e.g., TTG) (Fig. 9).

6. Discussion

6.1. Geochemical character, age and likely petrogenesis

As stated above, most samples from the Daxigou granitoids exhibit the mineralogical and geochemical characteristics of I-type granites. Most samples belong to the calc-alkaline series, are fairly rich in SiO_2, Na_2O ($Na_2O/K_2O > 1$ by weight) and have a metaluminous to subaluminous composition. The MgO (0.24–1.66 wt. %) concentrations are obviously lower than those in the average upper crust (2.48 wt. %; Rudnick and Gao 2003), and this precludes their derivation directly from the mantle. Furthermore, the relatively high alkalis suggest the presence of feldspars and/or biotite in the source (Jiang et al. 2005; Zhao XF et al. 2008). The high LREE/HREE ratios, high Sr contents and Sr/Y ratios, low Yb and Y contents and HFSE (Nb, Ta, P and Ti) depletion indicate that the Daxigou granitoids were likely generated at great depths, with garnet ± apatite, zircon, ilmenite or rutile as the main residual phases. In addition, their low initial εHf(t) values (−7.16 to −5.03, Tab. 3) reveal a continental crustal source. Older Paleoproterozoic rocks (e.g., the Xingditage Complex) can be ruled out as a source on the basis of geochemistry (low SiO_2) and isotopic characteristics (positive εHf(t): Long et al. 2010). A plausible source would represent Archaean rocks, exposed to the west of the Kuluketage Block, e.g., in the Tuoge Complex (2.65–2.75 Ga, Long et al. 2011a). Indeed, the T_{DM2} Hf model ages of the Daxigou granitoids and those for the Tuoge Complex are comparable.

In the Nb–Y diagram (Fig. 10a), all of the Daxigou granitoids fall in the field of the volcanic-arc or syn-collisional granites. However, in the Rb–(Yb + Nb) diagram (Fig. 10b), almost all of the data plot in the volcanic-arc field. As further evidence, all samples are depleted in Nb, which is typical of granitoids with arc affinity (e.g., Pearce et al. 1984) (Fig. 7b). In all, the combination of field investigations, whole-rock geochemical data, U–Pb ages and zircon Hf isotope data imply that the Daxigou granitoids represent the continental-arc I-type granites, which may have originated by remelting of the TTG (Tuoge Complex) materials.

6.2. Tectonic implications

The age and petrogenesis of the host granitoids have been one of main problems since the discovery of the Daxigou iron–phosphate deposit in the Kuluketage Block. We interpret the newly obtained age of 1830 ± 12 Ma in terms of Paleoproterozoic crystallization of the Daxigou

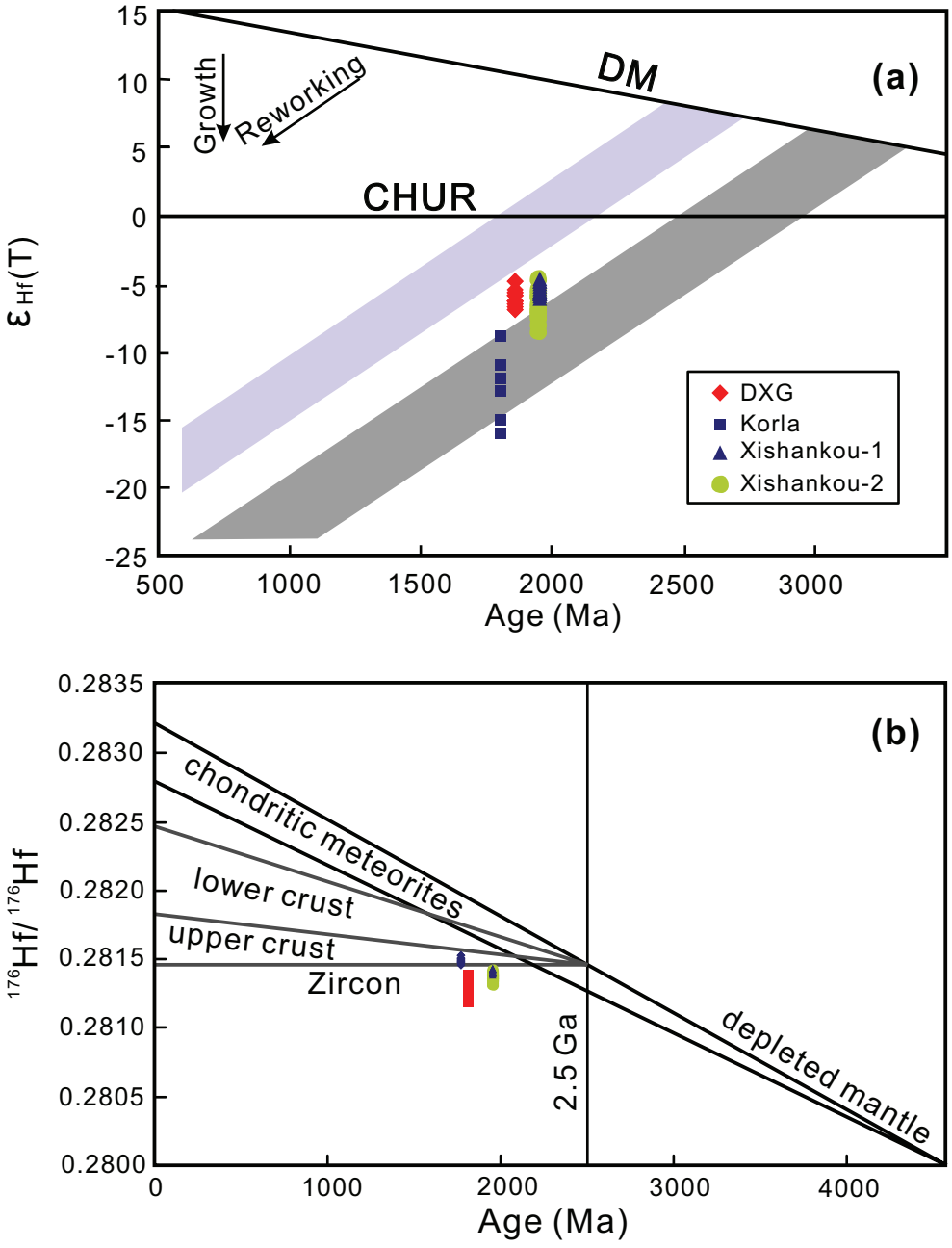

Fig. 9 Diagram of εHf(t)–age (**a**) and ($^{176}Hf/^{177}Hf$) ratios–age (**b**) for the syenogranite and related occurrences in the northern Tarim Craton. The purple and gray field in Fig. 9a represent the Neoarchaean and Mesoarchaean accretion-transformation, respectively. $^{207}Pb/^{235}U$ ages and εHf(t) values for the Korla Gneiss are from Long et al. (2010) and for the Xishankou-1 and Xishankou-2 (a Paleoproterozoic granitoid in Kuluketage Block) are from (Lei et al. 2012). DXG = Daxigou syenogranite. The data for the development of the main reservoirs are from Long et al. (2010).

granitoids. The zoning and chemistry of the dated zircons indicate their magmatic origin.

A series of high-precision ages of Tarim Craton basement rocks show that they have mainly experienced two major geological events: about 0.8–1.0 Ga (Zhu et al. 2008; Zhang et al. 2011; Cao et al. 2012) and 2.3–2.8 Ga (Zhang et al. 2012b; Zhang et al. 2013). However, our study indicates that the 1.8–2.0 Ga plutonism may have been important. In addition, the Mesoproterozoic Yangjibulake Group in Kuluketage, which shows effects of greenschist-facies metamorphism, unconformably overlies the Xinditage Group (Zhang et al. 2012a). Therefore, deducing an important tectonic event at the end of the Paleoproterozoic seems reasonable.

Some 1.9–1.8 Ga ages were recently documented at the margins of the Tarim Craton. However, most of these were ascribed to a metamorphic event (Zhang et al. 2012b). For instance, Wu HL et al. (2012) identified the existence of a 1.85 Ga metamorphic age peak from four metasedimentary rocks in Korla; Zhang et al. (2007b) described a *c.* 1.9 Ga metamorphic record from the Archaean gneiss and K-feldspar granite in southwestern Tarim and Zhang et al. documented *c.* 1.85–1.80 Ga metamorphic ages from Archaean TTG rocks and the

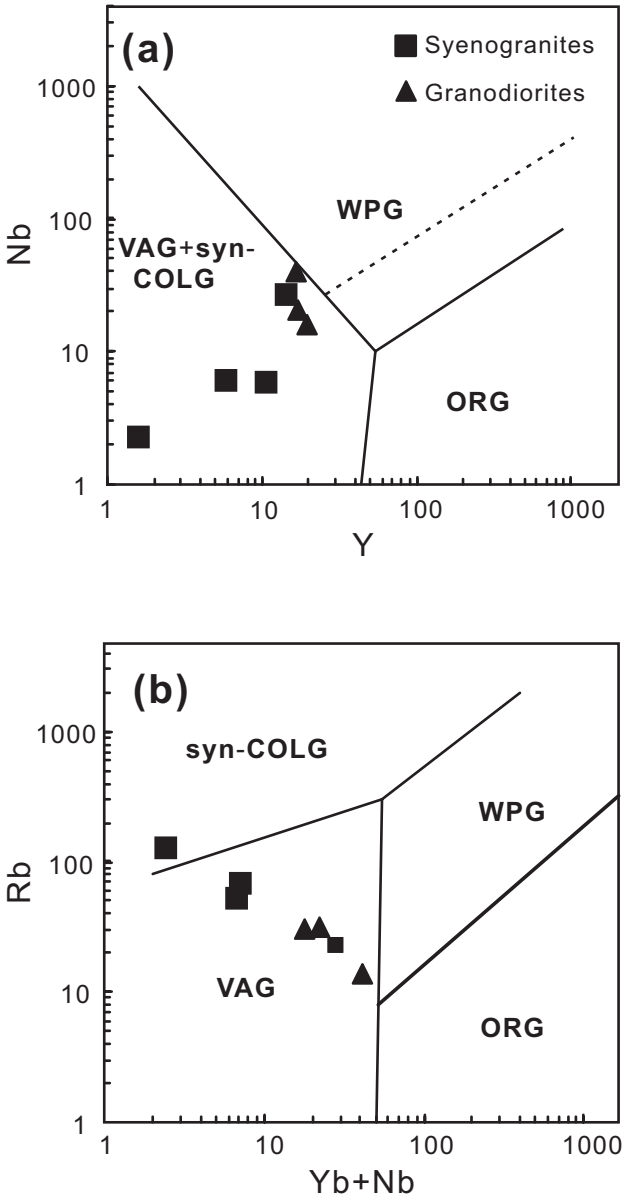

Fig. 10 Granite discrimination diagrams after Pearce et al. (1984): Nb–Y (**a**) and Rb–(Yb + Nb) (**b**). VAG: Volcanic Arc Granite; ORG: Ocean Ridge Granite; WPG: Within-Plate Granite; Syn-COLG: Syn--Collisional Granite; POG: Post-Collisional granite.

Paleoproterozoic metamorphic belt around Kuluketage (Zhang et al. 2012a).

Moreover, we have noticed that some tectono-magmatic events occurred there at 1.9–1.8 Ga, related to the assembly of Columbia Supercontinent. For instance, Zhang et al. (2007a) identified a 1987 ± 20 Ma inherited component in zircon grains from granodiorite north of Xingdi. Deng et al. (2008) obtained an age of 1916 ± 36 Ma by LA-ICP-MS zircon U–Pb dating of several inherited zircons from a gabbro in the Xingdi Valley of Kuluketage and Cao et al. (2010) an age of 1886 ± 61 Ma by LA-ICP-MS zircon U–Pb dating of several inherited zircon grains from Neoproterozoic K-feldspar granite of Dapingliang plutons. Recently, two igneous crystallization ages of 1934 ± 13 and 1944 ± 19 Ma from quartz diorite and granodiorite were obtained west of Kuluketage (Lei et al. 2012). However, the same authors stated that these zircons may have undergone high-temperature metamorphism, considering the nearly identical ages of the cores and metamorphic rims as well as their similar εHf(t) values. We can also see from the above ages that almost all of the zircons are either documented as metamorphic or inherited. In the current study, the 1830 ± 12 Ma age for the Daxigou syenogranite is thus the first reliable crystallization age of the Paleoproterozoic intrusive rocks in the Kuluketage Block.

Based on the above information, we infer an occurrence of an important Paleoproterozoic (*c.* 2.0–1.8 Ga) tectono-metamorphic and magmatic event in the Tarim Block. Late Paleoproterozoic collisional orogenic events have been increasingly recognised in Precambrian cratons worldwide and may have ultimately resulted in the formation of the Columbia Supercontinent (e.g., Rogers and Santosh 2002; Zhao GC et al. 2002, 2004; Santosh et al. 2007; Zhao GC et al. 2009; Chen and Xing 2013). Therefore, the Paleoproterozoic (*c.* 1.8–1.9 Ga) tectono-magmatic events documented in this study indicate that the Tarim Craton may have taken part in the assembly of the Columbia Supercontinent as well. Voluminous I-type granitic plutons have been traditionally considered to form at active continental margins related to oceanic crust subduction (Wilson 1989). Because our zircon dating yielded late Paleoproterozoic crystallization ages, a continental arc-type setting is suggested for the northern Tarim at *c.* 1830 Ma. However, obtaining detailed information about the subduction zone, e.g., its polarity and location of the ocean is currently a challenge because of scarce information on the Kuluketage Block. Much more work is required to reconstruct the plate tectonic history in the Tarim Craton.

7. Conclusions

We can draw the following conclusions from our new field, zircon U–Pb ages and geochemical data:

1. LA–ICP-MS U–Pb zircon dating indicates that the emplacement and alteration of the Daxigou syenogranite occurred at 1830 ± 12 Ma and 1798 ± 21 Ma, respectively. This is the first record of a late Paleoproterozoic to early Mesoproterozoic magmatic event in the Kuluketage area.
2. Based on a combination of field investigations and petrographic, geochronological and geochemical evidence, we suggest that Daxigou granitoids belong to Paleoproterozoic continental-arc I-type granites, which may have originated by melting of Neoarchaean TTG (Tuoge Complex) materials.

3. The available data, together with previous studies, demonstrate that a Paleoproterozoic (*c.* 2.0–1.8 Ga) tectono-magmatic event occurred in the Kuluketage Block. We suggest a continental arc-type tectonic setting in the Kuluketage Block at late Paleoproterozoic times (*c.* 1830 Ma). The Tarim Craton may have participated in the assembly of the Columbia Supercontinent.

Acknowledgements. This paper benefited from an insightful and helpful review of Editor-in-chief Vojtěch Janoušek. We also acknowledge Milan Kohút for careful editing and valuable comments to the revised manuscript. Critical and constructive comments by two anonymous reviewers were of great help in improving the manuscript. We are grateful to Zheng Han, Hu Zhao-chu and Tang Wen-xiu of the State Key Laboratory of Geological Processes and Mineral Resources, China University of Geosciences, Wuhan, for their assistance in LA-ICP-MS and Hf isotope determinations. All thanks go to Shi Ran for her assistance during the experiments. Geology engineer Xi Guo-qing is acknowledged for leading the field work. This research was founded by the 305 Project of State Science and Technology Support Program (Grant No. 2011BAB06B04-05) as well as the China Postdoctoral Science Foundation projects (Grant No. 2012M521492 and 2013T60758).

References

Blichert-toft J, Albarède F (1997) The Lu–Hf isotope geochemistry of chondrites and the evolution of the mantle–crust system. Earth Planet Sci Lett 148: 243–258

Cao XF, Lv XB, Lei JH, Chen C, Wang YQ, Du BF, Mei W, Gao X, Du AD (2010) The age of the Neoproterozoic Dapingliang skarn copper deposit in Kuruketage, NW China. Resour Geol 60: 397–403

Cao XF, Lv XB, Liu ST, Zhang P, Gao X, Chen C, Mo YL (2011) LA-ICP-MS zircon dating, geochemistry, petrogenesis and tectonic implications of the Dapingliang Neoproterozoic granites at Quruqtagh Block, NW China. Precambr Res 186: 205–219

Cao XF, Gao X, Lv XB, Qin Q, Liu ST, Chen C, Guo RQ, Zhang B, Hu QT (2012) Sm–Nd geochronology and geochemistry of a Neoproterozoic gabbro at Kuluketage, north-western China. Int Geol Rev 54: 861–875

Chappell BW, White AJR (1974) Two contrasting granite types. Pac Geol 8: 173–174

Chappell BW, White AJR (1992) I- and S-type granites in the Lachlan Fold Belt. Trans Roy Soc Edinb, Earth Sci 83: 1–26

Chappell BW (1999) Aluminium saturation in I- and S-type granites and the characterization of fractionated haplogranites. Lithos 46: 535–551

Chen ZH, Xing GF (2013) Petrogenesis of a Paleoproterozoic S-type granite, central Wuyishan Terrane, SE China: implications for early crustal evolution of the Cathaysia Block. Int Geol Rev 55: 1445–1461

Cheng YQ (1994) Outline of Regional Geology in China. Geological Publishing House, Beijing, pp 1–517 (in Chinese with English abstract)

Condie KC (1989) Plate Tectonics and Crustal Evolution, 3rd edition. Pergamon Press, Elmsford, NY, pp 1–476

Condie KC (Ed) (1994) Archean Crustal Evolution. Elsevier, Amsterdam, pp 1–528

Corfu F, Hanchar JM, Hoskin PWO, Kinny P (2003) Atlas of zircon textures. In: Hanchar JM, Hoskin PWO (eds) Zircon. Mineralogical Society of America and Geochemical Society Reviews in Mineralogy and Geochemistry 53, Washington, pp 469–503

Demoux A, Kröner A, Liu DY, Badarch G (2009) Precambrian crystalline basement in southern Mongolia as revealed by SHRIMP zircon dating. Int J Earth Sci 98: 1365–1380

Deng XL, Shu LS, Zhu WB, Ma DS, Wang B (2008) Precambrian tectonism, magmatism, deformation and geochronology of igneous rocks in the Xingdi Fault zone, Xinjiang. Acta Petrol Sin 24: 2800–2808 (in Chinese with English abstract)

Feng BZ, Zhou YW, Peng QM, Chi SF, Jiang QG, Liu ZY, Xing LX, Yang TQ, Ye SQ (1995) Pre-Sinian Geology, Precious and Nonferrous Metal Deposits in Kuruketage Area, Xinjiang Uygur Autonomous Region, China. Geological Publishing House, Beijing, pp 1–282 (in Chinese with English abstract)

Gao ZJ, Chen JB, Lu SN, Peng CW, Qin ZY (1993) The Precambrian Geology in northern Xinjiang. Geological Publishing House, Beijing, pp 1–171 (in Chinese with English abstract)

Gerdes A, Zeh A (2009) Zircon formation versus zircon alteration – new insights from combined U–Pb and Lu–Hf in-situ LA-ICP-MS analyses, and consequences for the interpretation of Archean zircon from the Central Zone of the Limpopo Belt. Chem Geol 261: 230–243

Griffin WL, Pearson NJ, Belousova E, Jackson SE, Van-Achterbergh E, O'Reilly SY, Shee SR (2000) The Hf isotope composition of cratonic mantle: LAM-MC-ICP-MS analysis of zircon megacrysts in kimberlites. Geochim Cosmochim Acta 64: 133–147

Guo ZJ, Zhang ZC, Liu SW, Li HM (2003) U–Pb geochronological evidence for the early Precambrian complex of the Tarim Craton, NW China. Acta Petrol Sin 19: 537–542 (in Chinese with English abstract)

Hanchar JM, Rudnick RL (1995) Revealing hidden structures: the application of cathodoluminescence and back-scattered electron imaging to dating zircons from lower crustal xenoliths. Lithos 36: 289–303

Hawkesworth CJ, Kemp AIS (2006) Evolution of the continental crust. Nature 443: 811–817

Hoskin PWO, Black LP (2000) Metamorphic zircon formation by solid-state recrystallization of protolith igneous zircon. J Metamorph Geol 18: 423–439

Hu AQ, Wang ZG, Tu GC (1997) Geological Evolution, Petrogenesis and Metallogeny of North Xinjiang. Science Press, Beijing, pp 1–246 (in Chinese with English abstract)

Hu AQ, Zhang QF, Zhang GX (1999) Age and crustal growth of the basement of Tienshan Orogenic Belt: constraints from Nd isotope compositions. Sci China Ser D 29: 104–122 (in Chinese with English abstract)

Hu AQ, Jahn BM, Zhang GX, Chen YB, Zhang QF (2000) Crustal evolution and Phanerozoic crustal growth in northern Xinjiang: Nd isotopic evidence. Part I. Isotopic characterization of basement rocks. Tectonophysics 328: 15–51

Hu AQ, Wei GJ (2006) On the age of the Neoarchean Qingir gray gneisses from the northern Tarim Basin, Xinjiang, China. Acta Geol Sin 80: 126–134 (in Chinese with English abstract)

Hu ZC, Liu YS, Gao S, Liu WG, Zhang W, Tong XR, Lin L, Zong KQ, Li M, Chen HH, Zhou L, Yang L (2012) Improved in situ Hf isotope ratio analysis of zircon using newly designed X skimmer cone and jet sample cone in combination with the addition of nitrogen by laser ablation multiple collector ICP-MS. J Anal Atom Spectrom 27: 1391–1399

Jiang YH, Ling HF, Jiang SY, Fan HH, Shen WZ, Ni P (2005) Petrogenesis of a late Jurassic peraluminous volcanic complex and its high-Mg, potassic, quenched enclaves at Xiangshan, southeast China. J Petrol 46: 1121–1154

Lei RX, Wu CZ, Chi GX, Chen G, Gu LX, Jiang Yh (2012) Petrogenesis of the Palaeoproterozoic Xishankou Pluton, northern Tarim Block, northwest China: implications for assembly of the supercontinent Columbia. Int Geol Rev 54: 1829–1842

Li XH, Long WG, Li QL, Liu Y, Zheng YF, Yang YH, Chamberlain KR, Wan DF, Guo CH, Wang XC, Tao H (2010) Penglai zircon megacryst: a potential new working reference for microbeam analysis of Hf–O isotopes and U–Pb age. Geostand Geoanal Res 34: 117–134

Liu YS, Hu ZC, Gao S, Günther D, Xu J, Gao CG, Chen HH (2008) In situ analysis of major and trace elements of anhydrous minerals by LA-ICP-MS without applying an internal standard. Chem Geol 257: 34–43

Liu YS, Gao S, HU ZC, Gao CG, Zong K, Wang D (2010) Continental and oceanic crust recycling-induced melt–peridotite interactions in the Trans-North China Orogen: U–Pb dating, Hf isotopes and trace elements in zircons of mantle xenoliths. J Petrol 51: 537–571

Long XP, Yuan C, Sun M, Zhao GC, Xiao WJ, Wang YJ, Yang YH, Hu AQ (2010) Archean crustal evolution of the northern Tarim Craton, NW China: zircon U–Pb and Hf isotopic constraints. Precambr Res 180: 272–284

Long XP, Yuan C, Sun M, Xiao WJ, Zhao GC, Zhou KF, Wang YJ, Hu AQ (2011a) The discovery of the oldest rocks in the Kuluketage area and its geological implications. Sci China Ser D 54: 342–348

Long XP, Yuan C, Sun M, Kröner A, Zhao GC, Wilde S, Hu AQ (2011b) Reworking of the Tarim Craton by underplating of mantle plume-derived magmas: evidence from Neoproterozoic granitoids in the Kuluketage area, NW China. Precambr Res 187: 1–14

Lu SN, Yu H, Zhao F, Jin W (2002) Preliminary Study of Precambrian Geology in the North Tibet–Qinghai Plateau. Geological Publishing House, Beijing, pp 21–122 (in Chinese with English abstract)

Lu SN, Li HK, Zhang CL, Niu GH (2008) Geological and geochronological evidence for the Precambrian evolution of the Tarim Craton and surrounding continental fragments. Precambr Res 160: 94–107

Ludwig KR (2003) Isoplot/Ex version 3.00. A Geochronological Toolkit for Microsoft Excel, User's Manual. Berkeley Geochronology Center Special Publications No. 4, pp 1–70

Luo XR, Shi FP, Fan WD, Luo XT (2007) Age and geochemistry of Neoproterozoic granite from Kuluketage in the north of Tarim, Xinjiang. Resour Surv Environ 28: 235–241 (in Chinese with English abstract)

Pearce JA, Harris NBW, Tindle AG (1984) Trace element discrimination diagrams for the tectonic interpretation of granitic rocks. J Petrol 25: 956–983

Peccerillo A, Taylor SR (1976) Geochemistry of Eocene calc-alkaline volcanic rocks from the Kastamonu area, northern Turkey. Contrib Mineral Petrol 58: 63–81

Rittmann A (1953) Magmatic character and tectonic position of the Indonesia Volcanoes. Bull Volcanol 14: 45–58

Rogers JJW, Santosh M (2002) Configuration of Columbia, a Mesoproterozoic supercontinent. Gondwana Res 5: 5–22

Rudnick RL (1995) Making continental crust. Nature 378: 573–578

Rudnick RL, Gao S (2003) Composition of the continental crust. In: Rudnick RL (ed) The Crust. Treatise on Geochemistry 3, Elsevier, Oxford, pp 1–64

Santosh M, Wilde SA, Li JH (2007) Timing of Paleoproterozoic ultrahigh-temperature metamorphism in the North China Craton: evidence from SHRIMP U–Pb zircon geochronology. Precambr Res 159: 178–196

Shand SJ (1943) Eruptive Rocks. D. Van Nostrand Co., New York, pp 1–360

Shu LS, Deng XL, Zhu WB, Ma DS, Xiao WJ (2010) Precambrian tectonic evolution of the Tarim Block, NW China: new geochronological insights from the Quruqtagh domain. J Asian Earth Sci 42: 774–790

Sláma J, Košler J, Condon D J, Crowley JL, Gerdes A, Hanchar JM, Horstwood MSA, Morris GA, Nasdala L, Norberg N, Schaltegger U, Schoene B, Tubrett MN, Whitehouse MJ (2008) Plešovice zircon – a new natural reference material for U–Pb and Hf isotopic microanalysis. Chem Geol 249: 1–35

Söderlund U, Patchett PJ, Vervoort JD, Isachsen CE (2004) The ^{176}Lu decay constant determined by Lu–Hf and U–Pb isotope systematics of Precambrian mafic intrusions. Earth Planet Sci Lett 219: 311–320

Sun BS, Huang JH (2007) Sm–Nd isotopic age of Qieganbulak ultrabasic–carbonatite Complex in Xinjiang,

China and its geological significance. Acta Petrol Sin 23: 1611–1616 (in Chinese with English abstract)

Sun SS, McDonough WF (1989) Chemical and isotopic systematics of oceanic basalt: implication for mantle composition and processes. In: Saunders AD, Morry MJ (eds), Magmatism in the Ocean Basins. Geological Society of London Special Publications 42: pp 313–345

Wang HL, Xu XY, He SP, Chen JL (2007) Map of Tianshan and adjacent area (1:1,000,000). Geology Publishing House, Beijing (in Chinese with English abstract)

Wang ZM, Han CM, Su BX, Patrick AS, Sanjeewa PKM, Ao SJ, Wang LJ (2013) The metasedimentary rocks from the eastern margin of the Tarim Craton: petrology, geochemistry, zircon U–Pb dating, Hf isotopes and tectonic implications. Lithos 179: 120–136

Wilson M (1989) Igneous Petrogenesis. Unwin Hyman, London, pp 1–466

Wolf MB, London D (1994) Apatite dissolution into peraluminous haplogranitic melts: an experimental study of solubilities and mechanism. Geochim Cosmochim Acta 58: 4127–4145

Woodhead JD, Hergt JM (2005) A preliminary appraisal of seven natural zircon reference materials for in situ Hf isotope determination. Geostand Geoanal Res 29: 183–195

Wu FY, Yang YH, Xie LW, Yang JH, Xu P (2006) Hf isotopic compositions of the standard zircons and baddeleyites used in U–Pb geochronology. Chem Geol 234: 105–126

Wu HL, Zhu WB, Shu LS, Zheng BH, He JW, Luo M (2012) Records of the assemblage event of Columbia Supercontinent in the Northern Tarim Craton. Geol J China Univ 18: 686–700

Xia XH, Yuan JZ, Xi GQ, Liang ZP (2010) Geochemistry of complex rocks and characteristics of Daxigou iron–phosphorite deposits, Xinjiang. J Jilin Univ (Earth Sci) 40: 879–886

Xiao WJ, Kusky T (2009) Geodynamic processes and metallogenesis of the Central Asian and related orogenic belts: introduction. Gondwana Res 16: 167–169

Xu B, Jiang P, Zheng HF, Zou HB, Zhang LF, Liu DY (2005) U–Pb zircon geochronology of Neoproterozoic volcanic rocks in the Tarim Block of northwest China: implications for the breakup of Rodinia supercontinent and Neoproterozoic glaciations. Precambr Res 136: 107–123

Xu B, Xiao SH, Zou HB, Chen Y, Li ZX, Song B, Liu DY, Zhou CM, Yuan XL (2009) SHRIMP zircon U–Pb age constraints on Neoproterozoic Quruqtagh diamictites in NW China. Precambr Res 168: 247–258

Yuan Q, Cao XF, Lv XB, Wang XD, Yang EL, Liu YG (2013) Neoproterozoic metallogenic specialization and significance of the basic–ultrabasic complex in Kuluketage, Xinjiang Province. Xinjiang Geol 31: 287–292 (in Chinese with English abstract)

Zhang CL, Li XH, Li ZX, Lu SN, Ye HM, Li HM (2007a) Neoproterozoic ultramafic–mafic–carbonatite complex and granitoids in Quruqtagh of northeastern Tarim Block, western China: geochronology, geochemistry and tectonic implications. Precambr Res 152: 149–169

Zhang CL, Li ZX, Li XH, Yu HF, Ye HM (2007b) An early Paleoproterozoic high-K intrusive complex in southwestern Tarim Block, NW China: age, geochemistry, and tectonic implications. Gondwana Res 12: 101–112

Zhang CL, Li ZX, Li XH, Ye HM (2009) Neoproterozoic mafic dyke swarm in north margin of the Tarim, NW China: age, geochemistry, petrogenesis and tectonic implications. J Asian Earth Sci 35: 167–179

Zhang CL, Xu YG, Li ZX, Wang HY, Ye HM (2010) Diverse Permian magmatism in the Tarim Block, NW China: genetically linked to the Permian Tarim mantle plume? Lithos 119: 537–552

Zhang CL, Yang DS, Wang HY, Takahashi Y, Ye HM (2011) Neoproterozoic mafic–ultramafic layered intrusion in Quruqtagh of northeastern Tarim Block, NW China: two phases of mafic igneous activity with different mantle sources. Gondwana Res 19: 177–190

Zhang CL, Li HK, Santosh M, Li ZX, Zou HB, Wang HY, Ye HM (2012a) Precambrian evolution and cratonization of the Tarim Block, NW China: petrology, geochemistry, Nd-isotopes and U–Pb zircon geochronology from Archaean gabbro–TTG–potassic granite suite and Paleoproterozoic metamorphic belt. J Asian Earth Sci 47: 5–20

Zhang CL, Li HK, Wang HY (2012b) A review on Precambrian tectonic evolution of Tarim Block: possibility of interaction between Neoproterozoic plate subduction and mantle plume. Geol Rev 58: 923–933 (in Chinese with English abstract)

Zhang CL, Zou HB, Li HK, Wang HY (2013) Tectonic framework and evolution of the Tarim Block in NW China. Gondwana Res 23: 1306–1315

Zhao GC, Cawood PA, Wilde SA, Sun M (2002) A review of the global 2.1–1.8 Ga orogens: implications for a pre-Rodinian supercontinent. Earth Sci Rev 59: 125–162

Zhao GC, Sun M, Wilde SA, Li S (2004) A Paleo–Mesoproterozoic supercontinent: assembly, growth, and breakup. Earth Sci Rev 67: 91–123

Zhao GC, He YH, Sun M (2009) The Xiong'er volcanic belt at the southern margin of the North China Craton: petrographic and geochemical evidence for its outboard position in the Paleo–Mesoproterozoic Columbia Supercontinent. Gondwana Res 16: 170–181

Zhao XF, Zhou MF, Li JW, Wu FY (2008) Association of Neoproterozoic A- and I-type granites in South China: implications for generation of A-type granites in a subduction-related environment. Chem Geol 257: 1–15

Zhu WB, Zhang ZZ, Shu LS, Lu HF, Sun JB, Yang W (2008) SHRIMP U–Pb zircon geochronology of Neoproterozoic Korla mafic dykes in the northern Tarim Block, NW China: implications for the long-lasting breakup process of Rodinia. J Geol Soc, London 165: 887–890